



Title	Uniaxial tension-compression fatigue behavior and fiber bridging degradation of strain hardening fiber reinforced cementitious composites
Author(s)	Matsumoto, Takashi; Wangsiripaisal, Kavalin; Hayashikawa, Toshiro; He, Xingwen
Citation	International Journal of Fatigue, 32(11), 1812-1822 <a href="https://doi.org/10.1016/j.ijfatigue.2010.04.012">https://doi.org/10.1016/j.ijfatigue.2010.04.012</a>
Issue Date	2010-11
Doc URL	<a href="http://hdl.handle.net/2115/45420">http://hdl.handle.net/2115/45420</a>
Type	article (author version)
File Information	IJF32-11_1812-1822.pdf



[Instructions for use](#)

Uniaxial tension-compression fatigue behavior and fiber bridging degradation of strain hardening fiber reinforced cementitious composites

Takashi Matsumoto<sup>a\*</sup>, Kavalin Wangsiripaisal<sup>b</sup>, Toshiro Hayashikawa<sup>a</sup>, Xingwen He<sup>a</sup>

<sup>a</sup> Division of Built Environment, Graduate School of Engineering, Hokkaido University, Sapporo, 060-8628, Japan

<sup>b</sup> Department of Civil Engineering, Graduate School of Engineering, University of Tokyo, Tokyo, 113-8656, Japan

\* Corresponding author. Division of Built Environment, Graduate School of Engineering, Hokkaido University, Sapporo, 060-8628, Japan Tel: +81-11-706-6171 Fax: +81-11-706-6172 Email: takashim@eng.hokudai.ac.jp

## Abstract

This study aims to clarify experimentally the uniaxial tension-compression fatigue behavior and fiber bridging stress degradation of strain hardening fiber reinforced cementitious composites. During fatigue cyclic loading, tensile bridging stress corresponding to the preset maximum tensile strain was recorded with the number of cycles in order to observe the degradation of the tensile bridging stress. Major bridging stress degradation was observed before reaching 1,000 cycles, and microscopic observation of the failure surface confirmed severe fiber damages. Fitting curves of bridging stress degradation are

proposed with the idea of Weibull distribution. The preliminary results of the current study with a limited number of specimens are compared with those of a uniaxial tensile fatigue study, and the differences of bridging stress degradations are discussed.

Keywords: Fiber reinforced material; Strain hardening; Fiber bridging; Strain controlled fatigue;

Compressive loading

## 1. Introduction

Fiber reinforced cementitious composites (FRCC) are increasingly applied to structural applications such as tunnel lining, pavement, overlay, bridge deck overlay, railroad sleepers, and factory floor slab (Horii et al. [1], Rizkalla and Mufti [2], Shirazi et al. [3], Strand et al. [4], Krstulovic-Opara et al. [5], Balaguru [6]). These applications utilize high strength, ductility, and crack resistance of FRCCs in tension, for the purpose of increasing the safety and durability of structures. It is well known that these beneficial properties are due to bridging fibers that transfer stresses across a crack. Since there are various kinds of fibers and choices of fiber dimensions in order to obtain suitable properties of an FRCC, it is important to understand a fiber bridging constitutive law which is the relation between fiber bridging stress and crack opening displacement (Li [7]).

In addition to conventional FRCCs, strain hardening fiber reinforced cementitious composites (SHFRCC) have been investigated recently (Kunieda and Rokugo [8]). This new class of material was developed with the micromechanical understanding of fiber bridging (Li and Leung [9]), and it acquires the following remarkable properties (Li [10], Li [11]). SHFRCC exhibits superior tensile properties to conventional FRCC. SHFRCC shows strain hardening behavior under tension, and its tensile strain can reach as high as 6 %. This high tensile strain capacity is due to the formation of distributed multiple fine cracks. Moreover, the width of multiple fine cracks remains below 100  $\mu\text{m}$  during the strain hardening

process, and this small crack width is beneficial for the increased durability of structures. These unique properties are made possible with relatively moderate amount of fibers: usually 2 vol. % of fibers. A typical composition includes cement, water, and sand with the ratio of 1:0.45: 0.5-1.2 (Li et al. [12]). Compared to conventional FRCCs, SHFRCC is a ductile and durable cementitious composite, and its properties are unique and superior.

With these superior properties, SHFRCC has been applied to various structures to date (Kunieda and Rokugo [8]). Examples include coupling beams of a reinforced concrete building for earthquake resistance and surface repair of a bridge and a retaining wall made of reinforced concrete against alkali silica reaction or carbonation. The former example utilizes the ductility of SHFRCC, while the latter utilizes the multiple fine cracks.

In addition to these applications, SHFRCC is finding applications to fatigue intensive structures. For example, it is reported that SHFRCC was applied to link slab of a bridge and also to patch repair of concrete pavement (Kim et al. [13], Li [14]). These applications are intended against traffic load, and the fatigue properties of SHFRCC are intended to be utilized. In order to secure the fatigue performance of SHFRCC structures, it is necessary to confirm that the superior properties of SHFRCC are not negated even under or after fatigue loads.

However, there are not many studies about the fatigue properties of SHFRCC. The fatigue properties of SHFRCC have been investigated so far under flexure and tension by a limited number of studies.

Flexural fatigue properties of SHFRCC have been investigated intensively by Suthiwarapirak et al. [15], Matsumoto et al. [16], and Suthiwarapirak et al. [17]. These studies conducted four point flexural fatigue tests on two types of SHFRCC in comparison with two types of polymer cement mortar and one type of steel fiber reinforced cement. The results showed that both SHFRCCs exhibited a unique fatigue stress-life relationship that is represented by a bilinear function on a semi-logarithmic scale, and that these materials exhibited higher fatigue strength in the comparison. Also, it was confirmed that the failure mechanisms of these SHFRCCs involved the development of multiple cracks that was followed by a localized crack at final fracture, although the development level of multiple cracks was dependent on fatigue stress level.

Tensile fatigue has been investigated by Matsumoto et al. [18] with the focus on bridging stress degradation. In the study, uniaxial tensile fatigue experiment was conducted under constant strain amplitude, unlike ordinary fatigue experiments under constant stress amplitude, and the degrading bridging stress was measured with the number of cycles. The resulting relation, hereinafter called bridging stress degradation, showed gradual decrease initially up to 1,000 cycles, sudden drop from 1,000 to 10,000 cycles, and ceasing around 10,000 cycles. It was also found that bridging stress degradation was due to the loss of fibers triggered by fiber fatigue rupture.

Based on the fatigue characteristics under flexure and tension, an analytical study also has been conducted by Suthiwarapirak and Matsumoto [19] with the concept of fiber bridging degradation. This

is a study that further developed the previous studies by Li and Matsumoto [20] and Matsumoto and Li [21]. The study employed finite element method to analyze the fatigue behavior of SHFRCC, and successfully reproduced fatigue crack propagation and subsequent fracture. Theoretically reproduced S-N diagrams and deformation behaviors showed a good agreement, supporting the validity of aforementioned studies.

All above fatigue studies were conducted either for flexure or tension. Those studies show that the tested SHFRCCs exhibit superior performances to FRCC, and that bridging stress degradation explains the fatigue behavior of SHFRCC. If cracks in structures are cyclically loaded under tension range, these studies support the usage of SHFRCC for fatigue intensive structures.

However, this may not be the case sometimes. In some structures, cracks can be cyclically loaded under tension and compression range. Tension-compression fatigue can be possible in members where fully reversed fatigue loads are present, and, in such a loading condition, more severe damages of SHFRCC can be expected. To date, this has not been investigated quantitatively.

Therefore, this study aims to clarify the behavior and degradation of SHFRCCs under uniaxial tension-compression fatigue loading. The experiment is conducted under constant strain amplitude that induces crack open, closure, and compression. The degrading bridging stress is measured with the number of cycles. The resulting bridging stress degradation of tension-compression fatigue will be compared with that of tensile fatigue, and the mechanisms of bridging stress degradation will be

discussed.

## 2. Tension-compression fatigue experiment

### 2.1 Materials and specimens

Static and fatigue specimens of SHFRCC that is reinforced with polyvinyl alcohol (PVA) fibers were fabricated. The properties of PVA fibers are shown in Table 1. In the experiment, two mixes were used, and their mix proportion is shown in Table 2. While Mix A included normal fine aggregates, Mix B replaced fine aggregates partially with light weight aggregates. The light weight aggregates are made of ceramic, and they have a balloon shape, i.e. empty inside. The purpose of Mix B is to reduce its matrix fracture toughness so that composite ductility can be enhanced. The compressive strength was measured: 46.5 MPa for Mix A and 38.0 MPa for Mix B.

Specimen dimensions are shown in Fig. 1. The specimen dimensions are designed in order to control the initiation of cracks in a specific area and to eliminate the overall failure of a specimen at or near the grip. Namely, the cross sectional area is gradually reduced from 100 mm square at both ends to 100 mm by 60 mm at the center, and it is constant over the central 100 mm length. Within this constant cross sectional zone, multiple cracks are intended to initiate and grow. At both ends, the cross sectional area is also constant in order to have bonding to loading grips. The total length of a specimen is 400 mm.

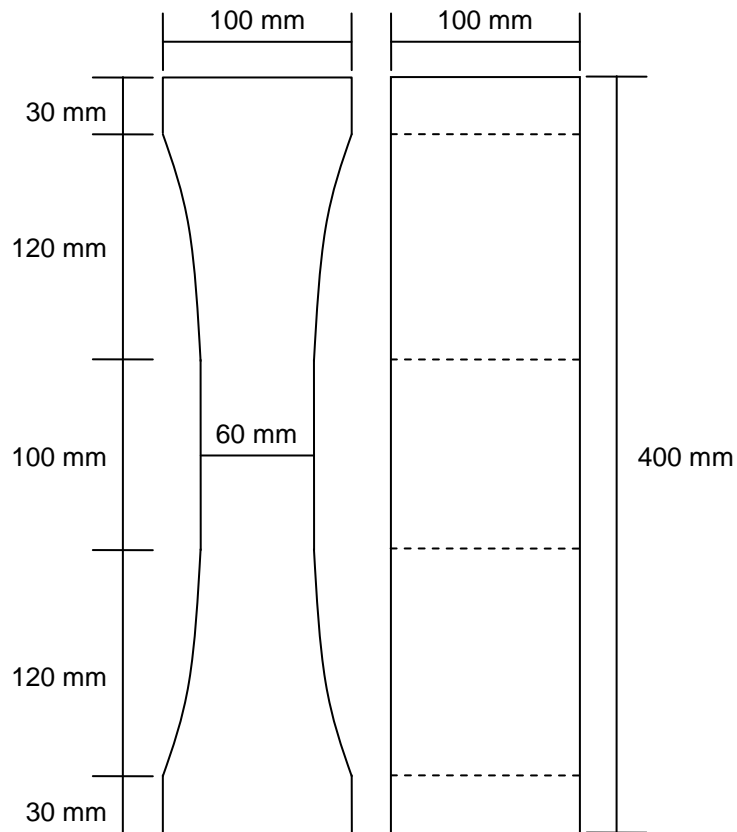


**Fig. 1. Shape and dimensions of specimens.**

The tested SHFRCC was made from a premix package, and the specimens were fabricated by a spraying method. First, all materials were prepared according to the mix proportions of Table 2. Second, admixtures were mixed with water, and premix of cement and PVA fibers were mixed in a mixer with the water including admixtures. Third, fresh SHFRCC was pumped into a spray gun, and it was sprayed into formworks. Finally, the surface of fresh specimens was leveled with a trowel. After the fabrication, all the specimens were demolded one day after, and they were cured under the constant temperature of 20 degrees Celsius. The age of specimens at either static or fatigue test was at least 28

days. In total, 13 specimens were prepared: 9 for Mix A and 4 for Mix B.

## 2.2 Experimental setup

Before the experimental setup, specimens were painted with a white color spray paint so that cracks could be identified and observed easily. Then, epoxy adhesive was used for bonding the ends of a specimen to upper and lower loading grip. The loading grip has four side plates with height of 50 mm in order to have enough stress-transferred area. Moreover, the plates are designed to have grooves so that mechanical bond works as well. Two to three hours were needed to gain enough bond strength between the grips and the specimen.

For data acquisition, four strain gauges were carefully attached with accurate alignment on the four side surfaces (Fig. 2). These gauges have 100 mm of gauge length, therefore they have enough length to cover the central constant cross sectional zone. These gauges were attached in order to measure the tensile and compressive strain over the central zone and to control the static and fatigue loading sequences under displacement control. In addition to the four strain gauges, load and stroke displacement were also obtained from the 200 kN capacity feed back controlled loading machine.

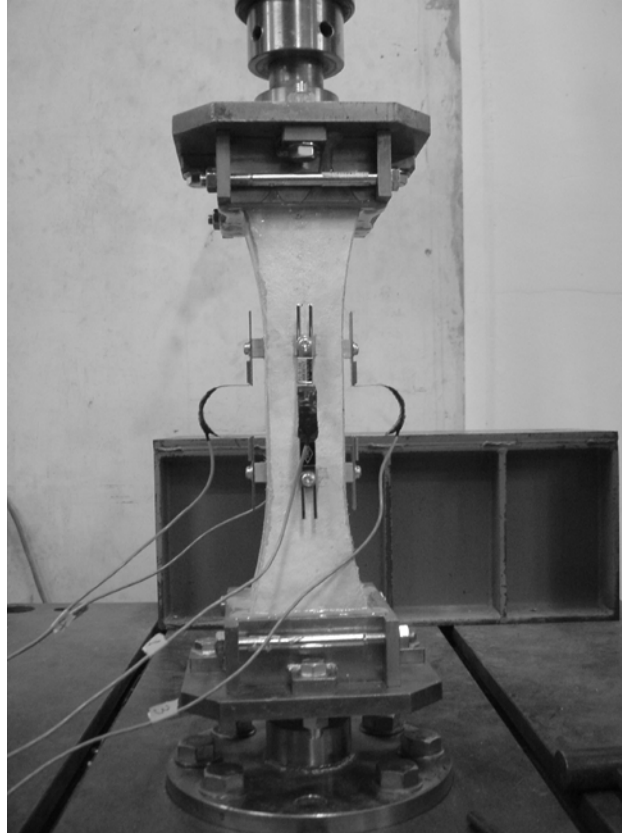


**Fig. 2. Experimental set-up. Strain gauge is attached on each of side surfaces.**

### 2.3 Experimental procedures

Procedures of static and fatigue experiments are explained in this section. Both of static and fatigue experiments were conducted under displacement control. The average strain value of four strain gauges was used to control the tensile loading of static specimens and the cyclic tension-compression loading of fatigue specimens.

There are three experimental cases as shown in Table 3. For Case 1 and 2, five Mix A specimens were tested under static tension. In Case 1, two Mix A specimens were tested under tension-compression

fatigue with maximum compressive strain 0.05 % and maximum tensile strain 0.2 %, while, in Case 2, two Mix A specimens with maximum compressive strain 0 % and maximum tensile strain 0.2 %. In Case 3, two Mix B specimens were tested under static tension, and two Mix B specimens under tension-compression fatigue with maximum compressive strain 0.05 % and maximum tensile strain 0.2 %. The reason why these strain values were chosen for fatigue will be explained later.

First, static tensile loading test was conducted. Loading was applied under displacement control at the rate of 0.005mm/sec. Load and the average of four gauges were recorded. Next, based on the static tensile loading test, the maximum tensile strain during fatigue loading was set to be 0.2 %. Also, two levels of maximum compressive strain during fatigue loading were selected: 0 % for Case 2 and 0.05 % for Case 1 and 3.

The former strain level of 0 % means that overall the specimens are not in compression, but it means that cracks are enforced to close fully (Fig. 3). As can be exemplified from visible cracks of unloaded fiber composite specimens (Matsumoto and Li [22], Wu et al. [23]), the cracks of unloaded specimens always have some remaining opening. This is because, even at overall zero load level, pulled-out fibers still remain in the crack and resist against the crack closure. Therefore, the maximum compressive strain level of 0 % means that there is no space between crack surfaces and that fibers have to be pushed back into matrix or to be buckled between crack surfaces. The latter strain level of 0.05 % is more severe than the former (Fig. 3). Not only fibers go back into matrix or buckle and crack surfaces are in

contact, but also fibers are compressed and crack surfaces are worn out.

The reason why these compressive strain levels were chosen is that, in some structural applications under traffic or temperature loading, cyclic fatigue loading into compression is possible to be present, although the usage of bridging fibers in compression is not advantageous.

Tension-compression fatigue loading was applied as follows (see also Fig. 3). First, a specimen was loaded in tension under displacement control at the rate of 0.005 mm/sec. After reaching the maximum tensile strain level, the specimen was unloaded, and further loaded into the maximum compressive strain level at the same rate of displacement control. From this point on, cyclic fatigue loading was applied at the frequency of 1 Hz under the constant displacement amplitude between the corresponding maximum tensile and compressive strain. Load and the average of four gauges were recorded. The cyclic loading was applied with a sinusoidal wave, and it was stopped when the load decrease ceased or the number of cycles reached 2,000 cycles.

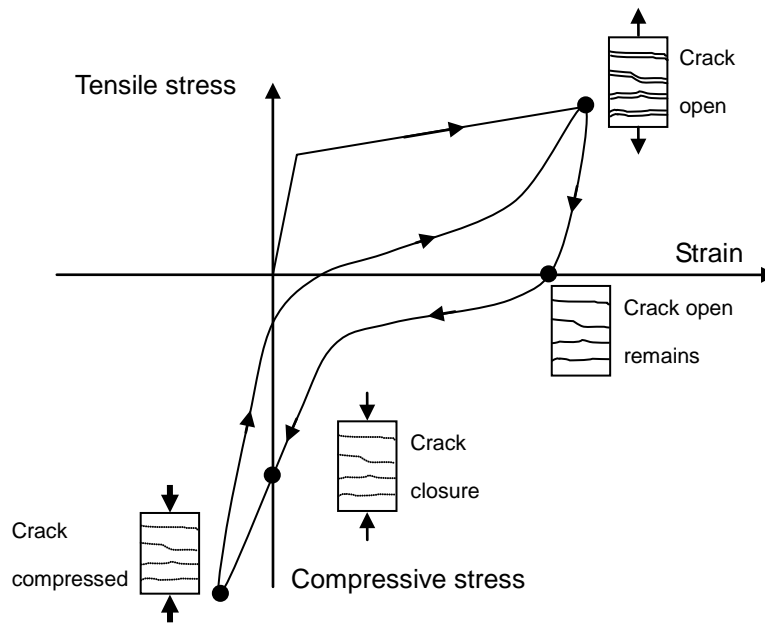


**Fig. 3. Tension-compression loading sequence and crack behaviors.**

### 3. Experimental results

#### 3.1 Static tensile test results

The obtained tensile stress-strain relations of Mix A are shown in Fig. 4, and those of Mix B in Fig. 5.

Tensile stress was observed to linearly increase with tensile strain, until first cracking took place.

Several load drops were observed, although they were recovered. These load drops were associated with

multiple crack occurrences during strain hardening. Finally, one of the cracks became localized, and

overall strain softening was observed. Since the final localization took place outside the gauge length in

a few specimens, those stress-strain curves exhibit unloading towards the origin. This explains the

variability of specimens shown in Figs. 4 and 5. Actually, multiple cracks were observed for all the

specimens.

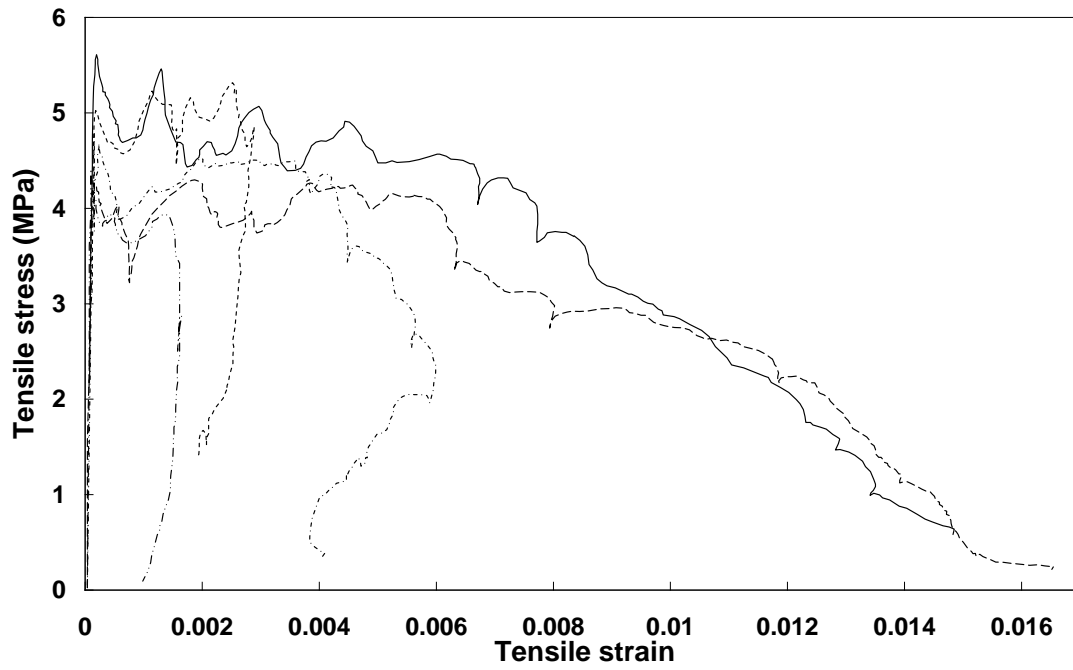
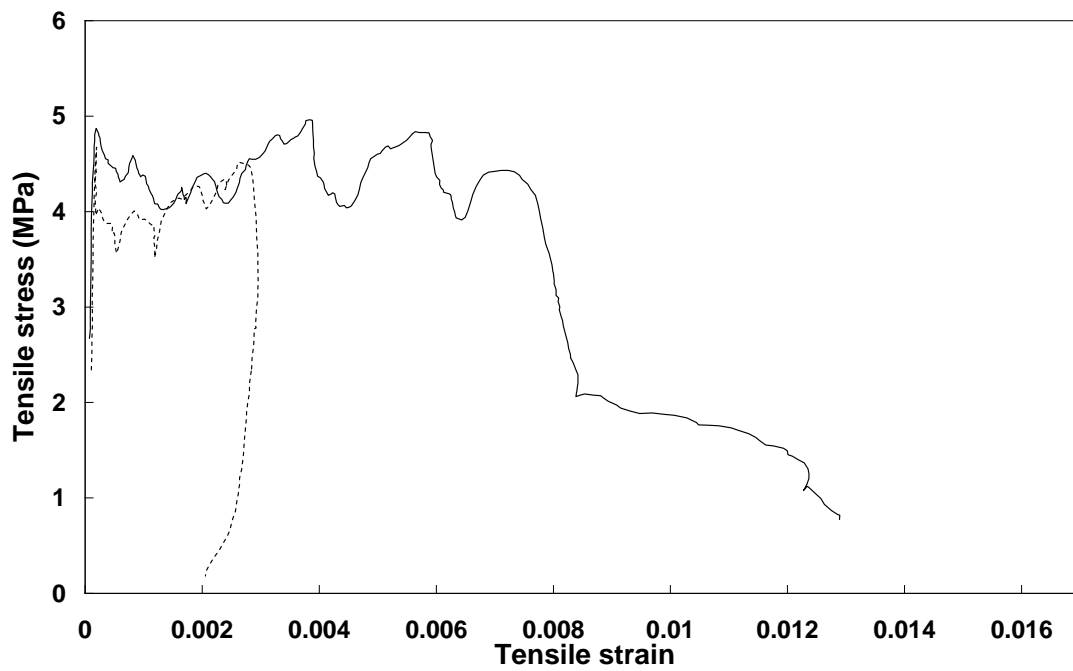


Fig. 4. Tensile behaviors of Mix A specimens.



**Fig. 5. Tensile behaviors of Mix B specimens.**

Both mixes showed strain hardening and multiple cracking that are the characteristics of SHFRCC.

The average tensile strength of Mix A is 4.98 MPa, and Mix B 4.83 MPa. The average tensile strain capacity measured at the first cracking stress level of Mix A is 0.414 %, and Mix B 0.375 %.

Fig. 6 shows the multiple cracks of Mix A and B, and it shows that these multiple cracks are mostly formed within the central zone. Mix B with light weight aggregates formed more cracks compared to Mix A, supporting the lowering effect of matrix fracture toughness by the light weight aggregates.

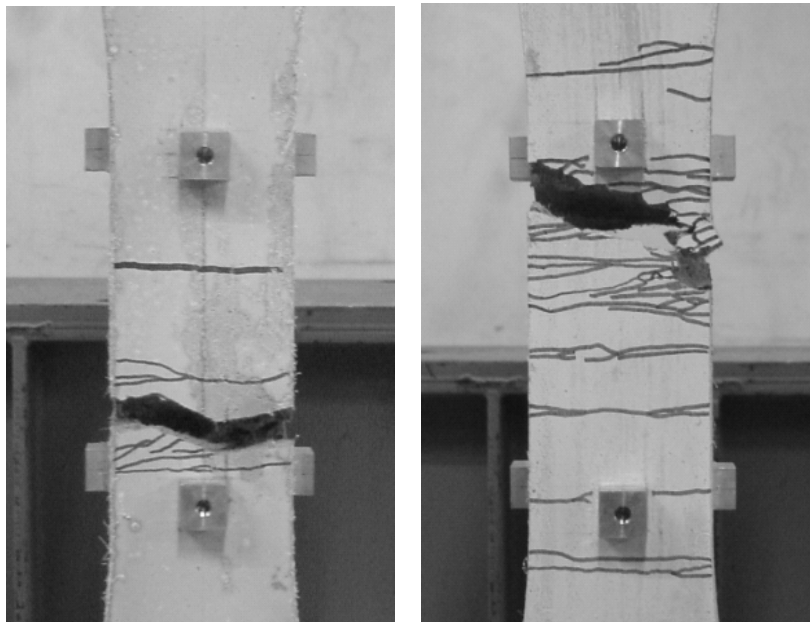


**Fig. 6. Multiple cracks of Mix A (left) and Mix B (right). Cracks are visualized with markings.**

### 3.2 Tension-compression fatigue test results

Based on the static tensile test, the maximum tensile strain during tension-compression fatigue test was set to be 0.2 %. This tensile strain level ensured that the specimens responded within strain hardening and did not go into strain softening. As mentioned previously, the tension-compression fatigue test was carried out under three loading cases depending on mixes and maximum compressive strain levels. In each case, two specimens were tested. This number of specimens is not enough, when the variability of fatigue life under the constant stress amplitude is considered. Therefore, in order to reduce the variability due to brittle failure, the maximum tensile strain level was set to be below the average strain capacity at the first cracking stress level measured in the static tensile test. This is because the fatigue test can be conducted in the strain hardening region that is related to progressive damage, not in the strain softening region that leads to localized failure. Also, the fatigue loading under constant strain amplitude leads to progressive damage, reducing the variability due to brittle failure.

Fig. 7 shows the hysteresis curves of a Case 1 specimen under tension-compression fatigue. The curves are the stress-strain behavior at first tensile loading, 1, 10, 100, and 1,000 cycles. From 1 to 100 cycles, the shapes of curves do not change significantly, and the maximum tensile and compressive stress on the curves decrease slightly. From 100 to 1,000 cycles, the curves change significantly. At 1,000 cycles, the tensile stress is nearly zero, meaning that a crack opens up with no tensile stress transmitted across the crack. The hysteresis curves imply that the bridging stress across the crack has degraded

quickly between 100 and 1,000 cycles.

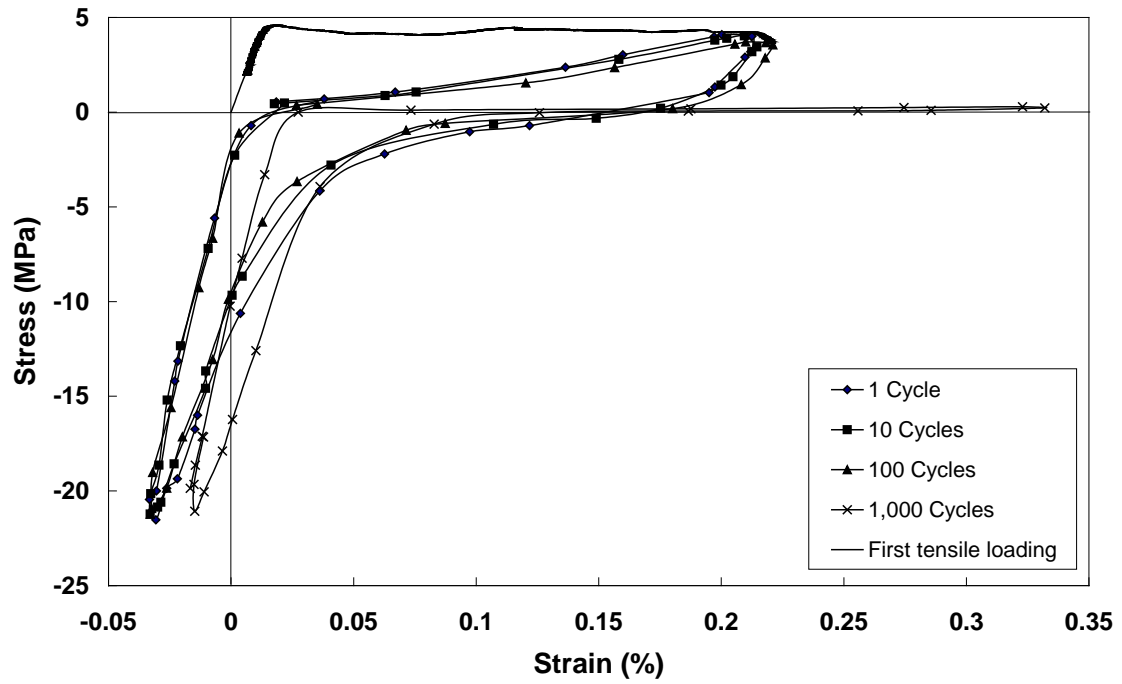
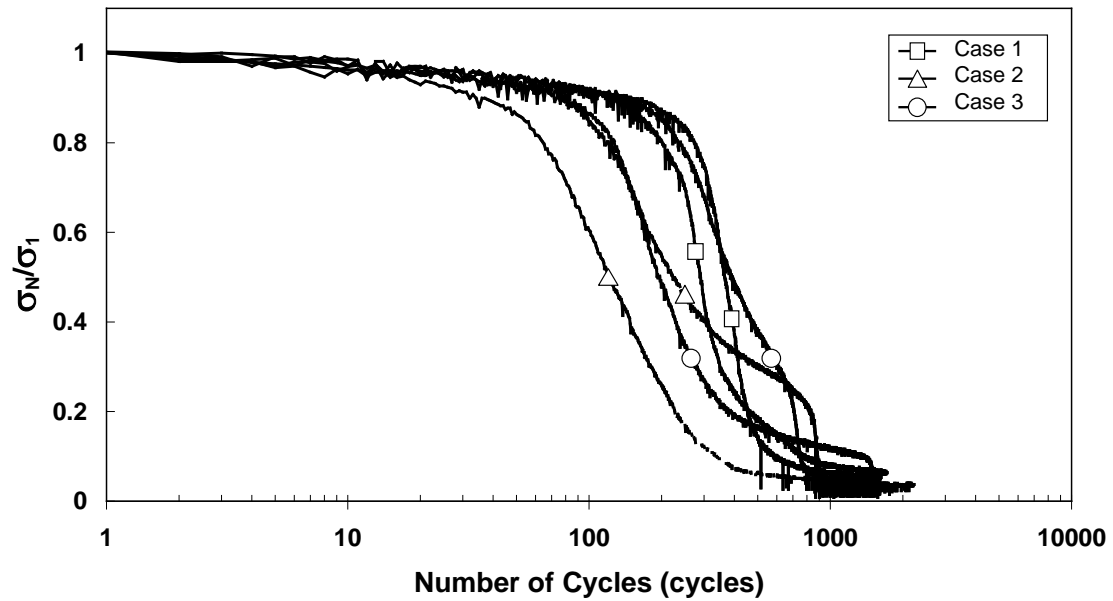


Fig. 7 Hysteresis curves during tension-compression fatigue of a Case 1 specimen.



**Fig. 8 Bridging stress degradation curves during tension-compression fatigue.**

In order to observe the bridging stress degradation, the tensile stress corresponding to the preset maximum tensile strain was recorded with the number of cycles. In Fig. 8, the ratio of the tensile stress at the current number of cycles,  $\sigma_N$ , to that at 1 cycle,  $\sigma_1$ , is plotted with the number of cycles for all the specimens. Fig. 8 shows that there are three stages in the bridging stress degradation curves. First, from 1 to 100 cycles, bridging stress gradually decreases roughly to 90 %. Second, from 100 to 1,000 cycles, the bridging stress sharply decreases roughly to 10 %. Some specimens suffer from severe damage, and those specimens exhibit a decrease nearly to 0 %. Finally, after the sharp decrease, the bridging stress decreases gradually again. The tests were terminated, if the final decrease is negligible and the number of cycles is above 1,000 cycles.

The differences among the experimental cases can be seen at the onset of the second stage and during the second stage.

For Case 1 and 2 of Mix A, Case 1 enters the second stage slightly later than Case 2, but Case 1 decays quickly with sharper gradients. This behavior was partially contrary to expectations. It was expected that Case 1 started to decay earlier and decayed quickly, since Case 1 was subjected to more severe loading conditions as explained in section 2.3. At this moment, the reason why Case 1 started to decay later than Case 2 is not clear.

Case 3 of Mix B started to decay earlier than Case 1, but later than Case 2. Also, Case 3 decays less quickly than Case 1, but more than Case 2. When compared to Case 1 under the same loading conditions, Case 3 exhibited more multiple cracks. The increased number of multiple cracks may contribute to the distribution of damages, and the gradient of the second decline stage in Case 3 might be achieved. The reason why Case 3 started to decay earlier than Case 1 is not clear at this moment.

Although there are not enough specimens to discuss the differences among the three cases, all the three cases show that the major bridging stress degradation takes place before 1,000 cycles and that the bridging stress degrades nearly to 10 %. It can be said that the bridging stress degradation under tension-compression fatigue is significantly severe, and that its degradation life on the order of  $10^3$  cycles is quite short compared to engineering design life on the order of  $10^6$  cycles.

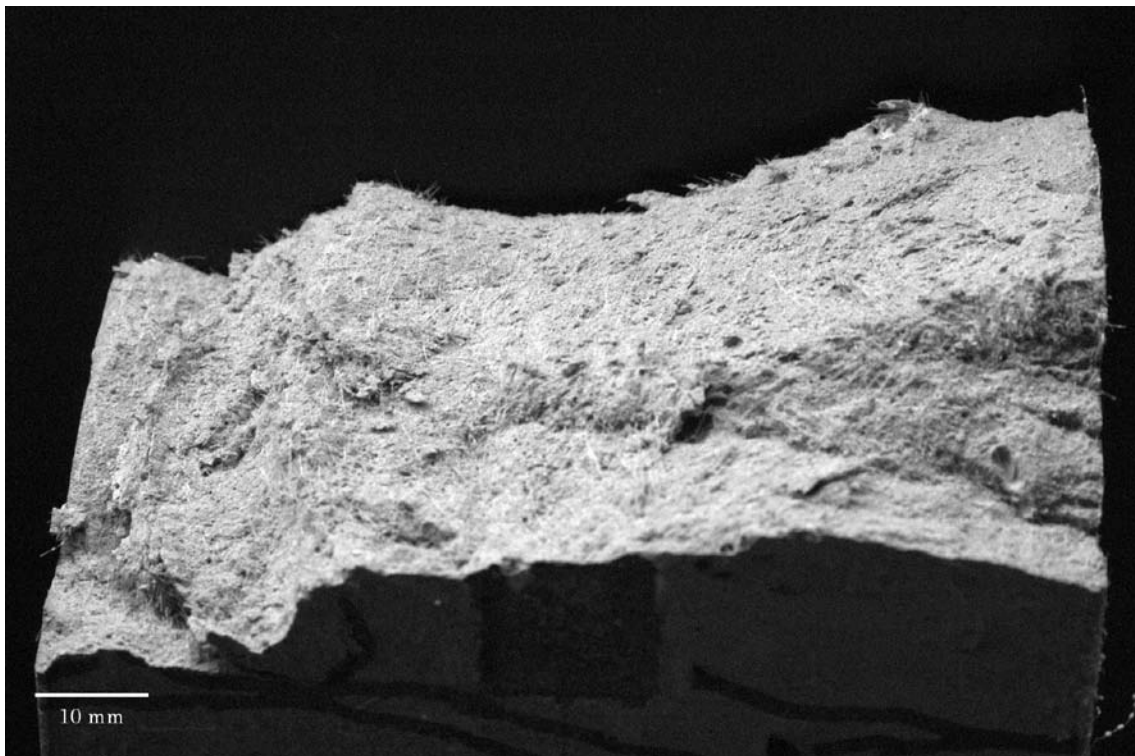
### 3.3 Failure surface observation after tension-compression fatigue tests

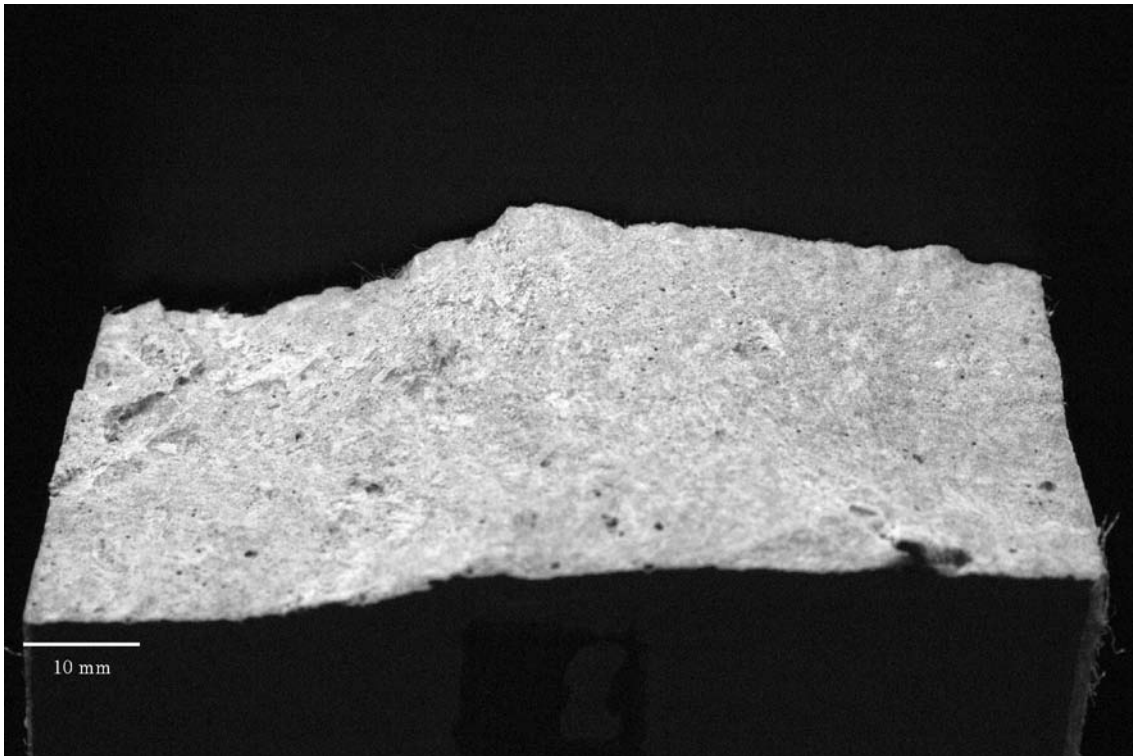
Failure surfaces of all the specimens were observed visually and with a digital microscope in order to understand the physical phenomena of fiber bridging stress degradation.

Fig. 9 shows the typical failure surfaces of a static specimen and a tension-compression fatigue (Case 1) specimen. Both specimens are made of Mix A. When the static specimen is compared to the fatigue specimen, it is clearly seen that the failure surface is rougher and that more fibers are protruded on the surface. Also, it was observed that cement powder accumulated on the failure surface of the fatigue specimen. The reason could be as follows. The failure surface in the fatigue specimen was made smooth, after the surface was subjected to cyclic contact and wear during tension-compression fatigue. At the same time, the fibers were damaged between the surfaces, and those fibers were worn out to short protrusion length. For further understanding of fiber damages, it is necessary to observe the fibers in situ under tension-compression fatigue, and detailed image analysis is required to examine the fiber failure mode.

Fig. 10 is a microscopic image of a crack. In the figure, a fiber is buckled, and other fibers are short-protruded on the surface. It is considered that some fibers are buckled between the crack surfaces under tension-compression fatigue, and that this buckling may lead to the rupture of fibers. Yielding is also possible for the rupture of fibers. In either case, it is considered that these ruptured fibers were worn out to the short protrusion length observed on the surface.

Fig. 9 and Fig. 10 exemplify the severity of tension-compression fatigue for bridging fibers. The early bridging stress degradation before 1,000 cycles obviously results from the severe damages to bridging fibers.





**Fig. 9 Failure surface of a static tensile specimen with protruded fibers (up) and a tension-compression fatigue (Case 1) specimen without protruded fibers (down).**



**Fig. 10 Buckling of a fiber and short protrusion of fibers.**

### 3.4 Curve-fitting to tension-compression fatigue test results

Fitting curves are obtained for the three cases of bridging stress degradation, and they are shown in Fig.

11, 12, and 13, respectively. The fitting curves are given by the following equation:

$$\frac{\sigma_N}{\sigma_1} = f(N) = g_1(N)w(N) + g_2(N)(1 - w(N)) \quad (1)$$

where

$$w(N) = \exp\left(-\left(\frac{\log N}{\log N_0}\right)^m\right), \quad (2)$$

$$g_1(N) = 1 - a_1 \log N, \text{ and} \quad (3)$$

$$g_2(N) = b_2 - a_2 \log N. \quad (4)$$

$w(N)$  is a Weibull distribution function where  $m$  is a shape parameter and  $\log N_0$  is a scale parameter.

$g_1(N)$  is a function that determines the initial slope of the curve, while  $g_2(N)$  is a function that determines the final slope of the curve. The coefficients,  $a_1$ ,  $a_2$ , and  $b_2$ , are to be determined in fitting, together with the two Weibull parameters.

Table 4 shows the parameters of the fitting curves. The shape parameter,  $m$ , of Case 1 is 25, while those of Case 2 and 3 are lower: 9 and 12, respectively. The shape parameter describes the gradient of the second decline stage of a bridging degradation curve. The larger the shape parameter is, the steeper the gradient becomes. Hence, with a large shape parameter like Case 1, the second decline stage can be narrowed down or well-defined. On the other hand, with a small shape parameter like Case 2 and 3, it has some range in two orders of magnitude. Regarding the scale parameter,  $\log N_0$ , it is noted that, when  $N$  is equal to  $N_0$ ,  $w(N)$  becomes  $1/e = 0.37$ , according to Weibull distribution. Namely,  $N_0$  points the number of cycles for the second decline stage.

The current curve-fitting relies mainly on Weibull distribution, but not only on it. The bridging stress

degradation takes place due to the gradual fatigue rupture of fibers. This gradual fatigue rupture results from the strength variability of fibers that has the nature of Weibull distribution.

However, in the current study, it is bridging stress that is measured with number of cycles, instead of survival probability. Since bridging stress is influenced by several factors in addition to the number of surviving fibers, its fitting curve can not be well expressed with Weibull distribution only. The noticeable differences are the initial and final slope.

These slopes are described by  $a_1$ ,  $a_2$ , and  $b_2$ .  $a_1$  and  $a_2$  are the gradient of the initial and final slope, and they are set to be the same. Case 1 shows slightly higher decline than Case 2 and 3. Physically, there can be some possible factors that are related to these slopes. First possibility is fiber relaxation, which leads to bridging stress decline even without fiber rupture. Second possibility is matrix damage. Aggregate bridging exerted across cracks can also be decreased under cyclic fatigue loading. Or microcracks can develop in the uncracked portion of matrix, and the stress transmitted to bridging fibers may decrease. Finally, matrix-fiber interface is also a possible source of these slopes. However, the interface damage is considered to be small and gradual. This is because, if the interface damage is significant, fibers are rather gradually pulled out, instead of ruptured.

$b_2$  is the intercept of the final slope, and it is set to be the same for all cases. It is considered that this parameter is related to the fibers cyclically loaded below fatigue limit. Below fatigue limit, these fibers exhibit virtually infinite life, and survive even after the second stage. Therefore, after the second stage,

the fitting curves approach the final slopes.

The currently obtained fitting curves well represent mechanical factors of fiber bridging degradation.

As the parameters and coefficients are obtained preliminary with two specimens for each case, they can

be made more accurate with the results of more specimens.

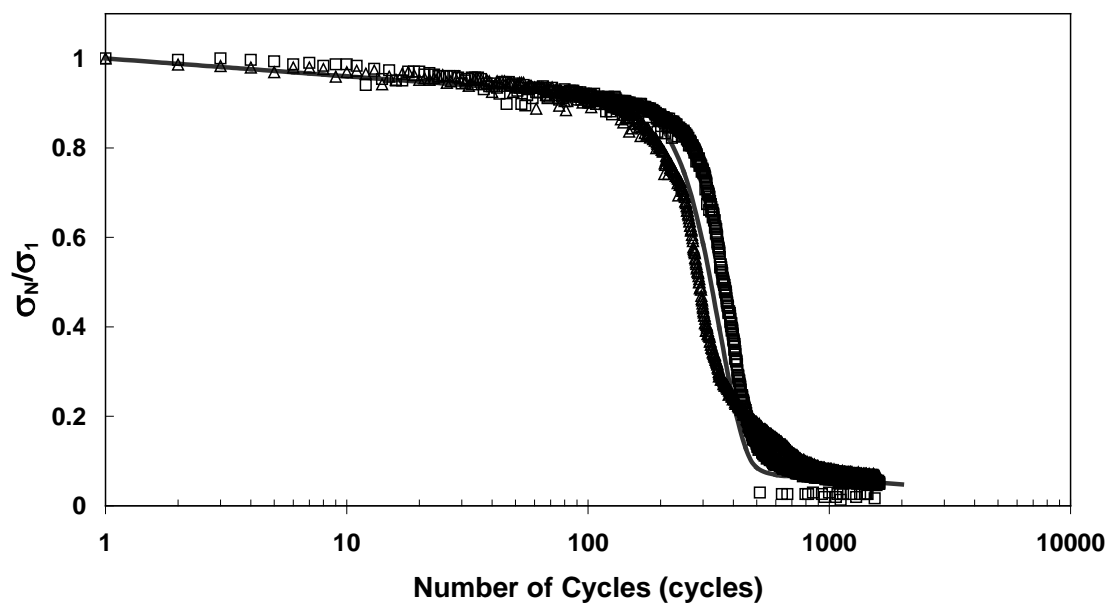


**Fig. 11** Fitting curve and bridging stress degradation curves of Case 1.

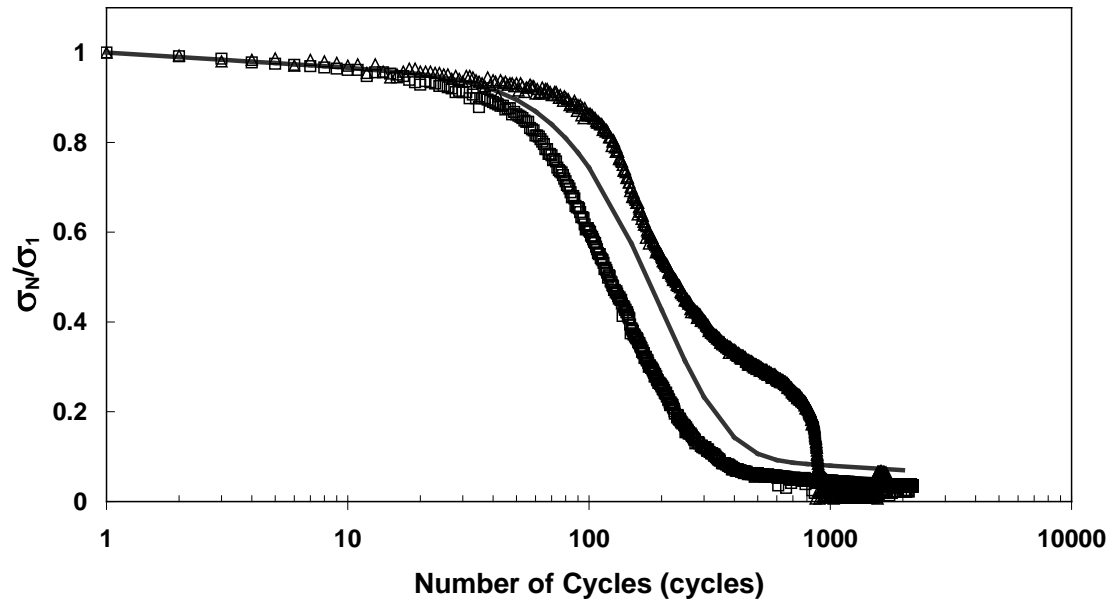


Fig. 12 Fitting curve and bridging stress degradation curves of Case 2.

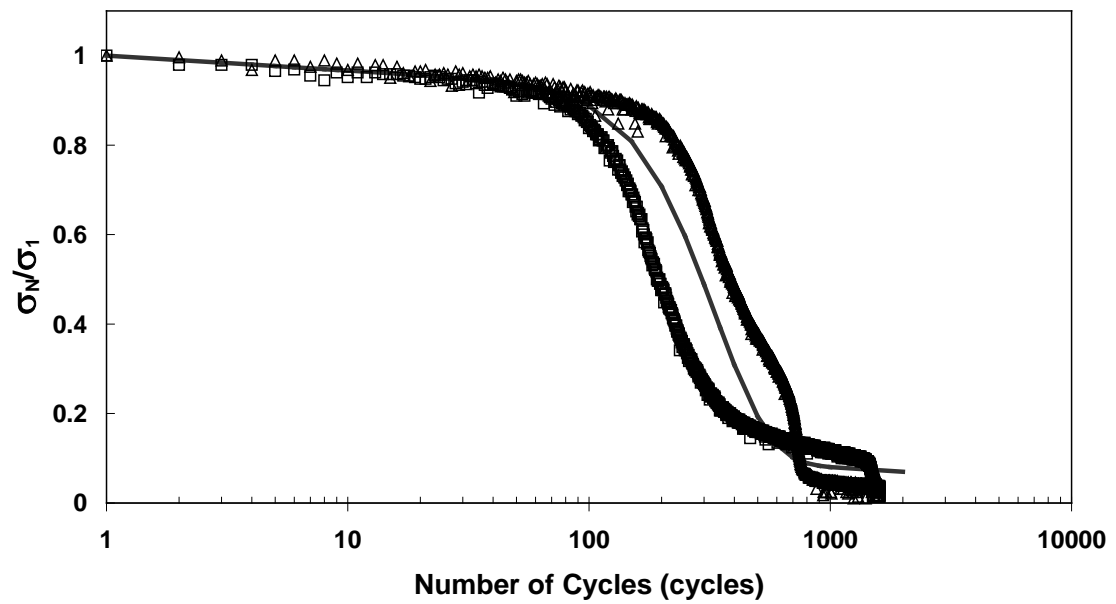


Fig. 13 Fitting curve and bridging stress degradation curves of Case 3.

## 4. Discussions

The current bridging stress degradation curves of tension-compression fatigue can be compared with those of tensile fatigue in Matsumoto et al [18]. The specimens tested under tensile fatigue were fabricated with a similar mix proportion. The tensile fatigue means that the specimens were cyclically loaded between maximum strain and minimum strain, where the maximum strain levels were 0.1, 0.15, or 0.2 %, while the minimum strain level was defined as the level where the load returns to zero. Unlike the current tension-compression fatigue, cracks still remain open even at the minimum strain level (see Fig. 3). The loading frequency was 4 Hz, and the loading pattern was sinusoidal.

Fig. 14, 15, and 16 show the resulting bridging stress degradation curves under tensile fatigue for the maximum strain level of 0.1, 0.15, and 0.2 %, respectively. The curves have similar behaviors to those presented in the current study. In the same manner, the curves can be divided into three stages.

Although the curves are similar qualitatively, they are quantitatively different. First, the initial gradual decrease continues to the level of 70~80 %, and this stage lasts for about a few thousands of cycles. The gradient of initial slope is rather steep compared to that of the current study. Second, the sharp decline takes place from the level of 70~80 % to 20~30 %. In the cited study, the amount of decrease is smaller, and the gradient of decrease is milder. The major difference is seen in the number of cycles. While the current study shows the order of  $10^2$  cycles, this cited study reports the order of  $10^4$  cycles. Finally, it is observed that the degradation slows down below the level of 20~30 %. In one

case, the level of bridging stress becomes nearly constant. This final level is higher than that of the current study.

Fig. 14, 15, and 16 also show the fitting curves obtained in the same way as explained in section 3.3, and Table 5 presents the parameters. The shape parameter,  $m$ , is smaller, meaning that the second decline stage has more range. The scale parameter,  $\log N_0$ , is larger, showing that the number of cycles for the second decline stage is larger. The gradient of the initial slope,  $a_1$ , is slightly steeper, although the loading condition is less severe in the cited study. This is probably because of the lack of measurement points from 1 to 1,000 cycles or the difference in matrix compositions. On the other hand, the gradient of the final slope,  $a_2$ , is set to be zero, based on the behaviors of the degradation curves. Finally, the intercept,  $b_2$ , is larger than that of the current study. This implies that, in the tensile fatigue condition, there are more fibers loaded below fatigue limit.

Physically, these differences arise from the loading conditions of bridging fibers. In the tensile fatigue, specimens achieve zero load level, but cracks remain open at zero load level. On the other hand, in the current tension-compression fatigue, specimens achieve zero strain level, and cracks are enforced to close. This is done by compressive loading. Furthermore, in Case 1 and 3, specimens are further loaded to compressive strain range, and fibers are loaded more severely. Namely, they are buckled and compressed between crack surfaces. This probably leads to a larger shape parameter, which means that fiber failure is less probabilistic and independent of the strength variability.

For further understanding of the phenomena, it is necessary to develop a micromechanical model which is based on microstructural parameters such as fiber length, fiber diameter, fiber modulus, fiber strength, etc. A model of this kind will clarify the influences of different loading conditions on bridging fibers and, in turn, on bridging stress degradation curves.

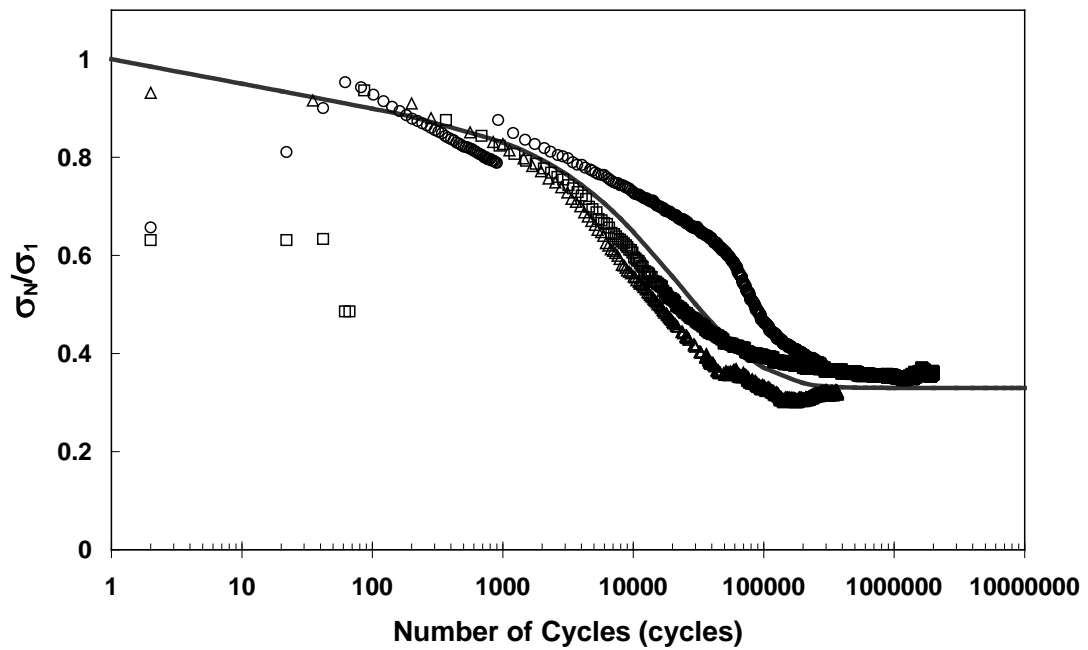


**Fig. 14 Fitting curve and bridging stress degradation curves during tensile fatigue with maximum tensile strain of 0.1 %.**

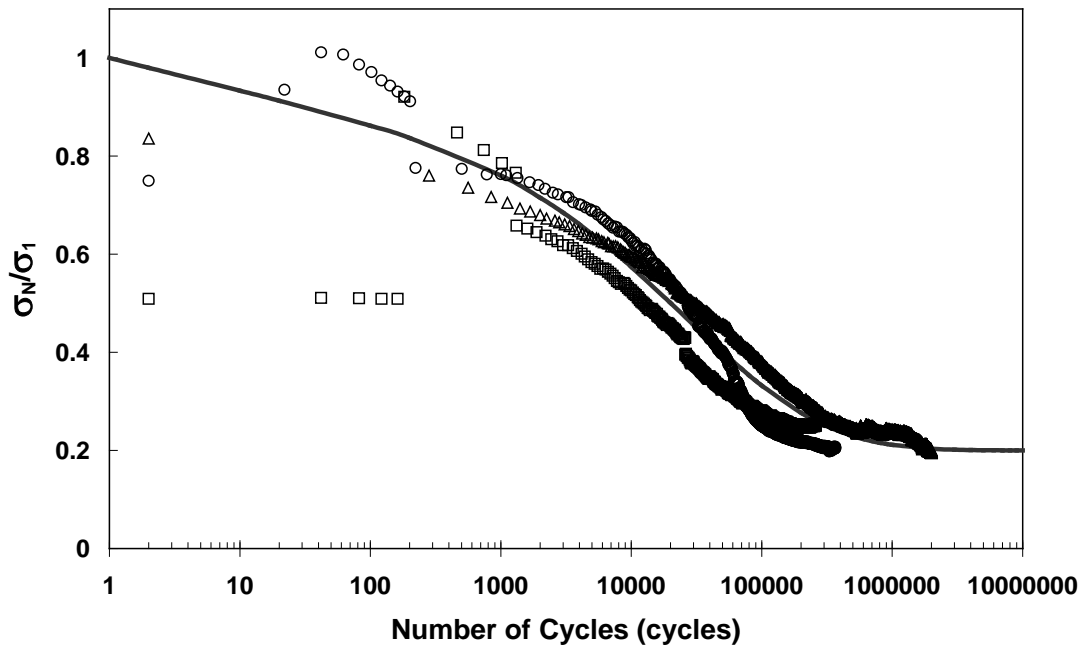


Fig. 15 Fitting curve and bridging stress degradation curves during tensile fatigue with maximum tensile strain of 0.15 %.

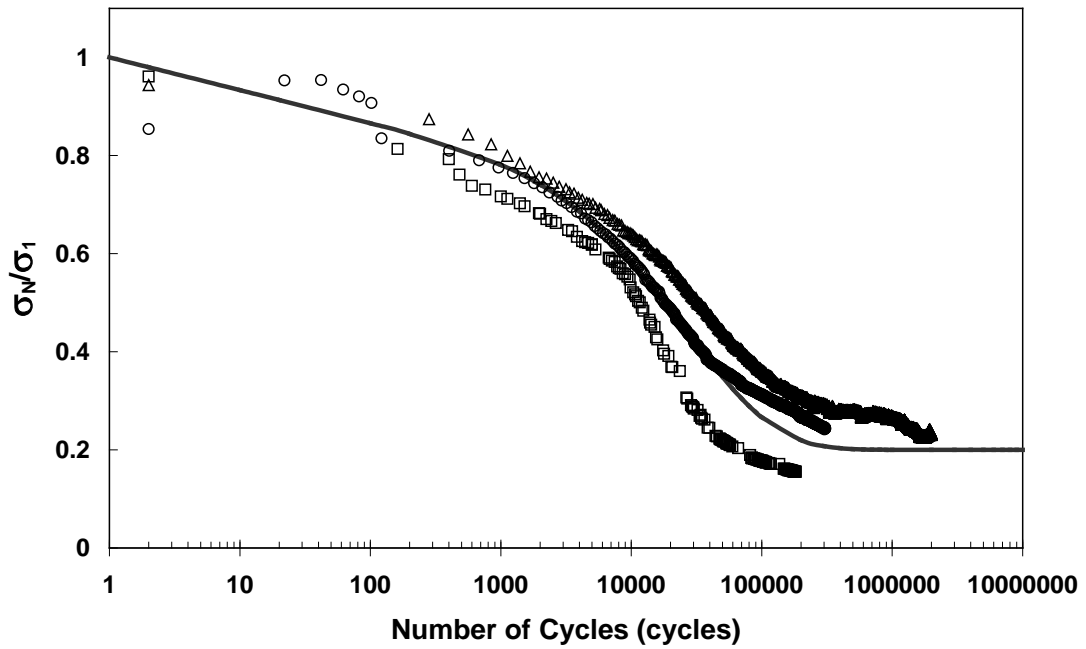


Fig. 16 Fitting curve and bridging stress degradation curves during tensile fatigue with

**maximum tensile strain of 0.2 %.**

## 5. Conclusions

This paper presented an experimental study of uniaxial tension-compression fatigue behavior and fiber bridging degradation of strain hardening fiber reinforced cementitious composites (SHFRCC).

SHFRCC specimens were cyclically loaded under constant strain amplitude, where the tensile strain during cyclic loading was 0.2 %, and the compressive strain was either 0 or 0.05 %. The hysteresis curves on the stress-strain plot were recorded, and the tensile stress corresponding to the tensile strain of 0.2 % was recorded with the number of cycles in order to observe the cycle-dependent degradation of fiber bridging stress.

It is found that bridging stress degradation happens in three stages. First, from 1 to 100 cycles, bridging stress decreases roughly to 90 %. Second, from 100 to 1,000 cycles, the bridging stress sharply decreases to about 10 %. Finally, after the sharp decrease, the bridging stress returns to gradual decrease. Although there are not enough specimens to discuss the differences among the three experimental cases, it is shown that the major bridging stress degradation takes place before 1,000 cycles, and that the bridging stress degrades to nearly 10 %. Visual observation identified that bridging fibers were severely damaged, and, after fatigue, no fibers were found to be protruded on the crack surface. This severe damage explains the significantly early and fast degradation of bridging stress.

Fitting curves are proposed based mainly on Weibull distribution. Weibull distribution describes the gradual fatigue rupture of fibers resulting from the strength variability. Additional terms to describe the gradual decrease of bridging stress in the initial and final stage are combined together with Weibull distribution. It has been shown that the proposed fitting curves well represent mechanical factors of fiber bridging degradation. As the parameters and coefficients are obtained preliminary with a limited number of specimens for each case, they can be made more accurate with the results of more specimens.

The current study is compared with a previous study which carried out uniaxial tensile fatigue of SHFRCC. Bridging stress degradation curves and their fitting curves are compared. It is found that the curves look similar, but that the degradation is significantly later and slower than that of the current study. This is probably because less number of fibers are buckled and none of them are pressed where the cracks still remain open even at the minimum strain level. Therefore, the fibers are less damaged.

For further understanding of the phenomena, it is necessary to conduct a series of experiments with sufficient number of specimens under various loading conditions and to perform the same analyses. Also, it is necessary to develop a micromechanical model which is based on microstructural parameters. A model of this kind will clarify the influence of different loading conditions on bridging fibers and, in turn, on bridging stress degradation curves.

## References

- [1] Horii H, Nanakorn P, Kabele P. Application of fracture mechanics to design of SFRC tunnel linings and development of strain-hardening cementitious composites. FRAMCOS-2: Proceedings of the Second International Conference on Fracture Mechanics of Concrete and Concrete Structures, Wittmann FH, editor. 1995, pp. 1345-1360.
- [2] Rizkalla SH, Mufti AA. Recent innovation for concrete highway bridges. Proceedings of ASCE 4th Materials Engineering Conference, Chong KP, editor. 1996, pp. 1063-1071.
- [3] Shirazi HH, Rasoulian M, King B. Design and construction of a bonded fiber concrete overlay of CRCP. Proceedings of ASCE 4th Materials Engineering Conference, Chong KP, editor. 1996, pp. 1647-1658.
- [4] Strand D, MacDonald CN, Ramakrishnan V, Rajpathak VN. Construction applications of polyolefin fiber reinforced concrete. Proceedings of ASCE 4th Materials Engineering Conference, Chong KP, editor. 1996, pp. 103-112.
- [5] Krstulovic-Opara N, Haghayeghi AR, Haidar M, Krauss PD. Use of conventional and high-performance steel-fiber reinforced concrete for bridge deck overlays. *ACI Materials Journal*, 1995;92(6): 669-677.
- [6] Balaguru PN, Shah SP. *Fiber-reinforced cement composites*. McGraw-Hill; 1992.
- [7] Li VC. Postcrack scaling relations for fiber reinforced cementitious composites. *Journal of Materials in Civil Engineering*, 1992;4(1):41-57.
- [8] Kunieda M, Rokugo K. Recent progress on HPRCC in Japan -Required performance and applications-.

- Journal of Advanced Concrete Technology, 2006;4(1):19-33.
- [9] Li VC, Leung CKY. Steady state and multiple cracking of short random fiber composites. Journal of Engineering Mechanics, 1992;188(11):2246-2264.
- [10] Li VC. From micromechanics to structural engineering -The design of cementitious composites for civil engineering applications. Journal of Structural Mechanics and Earthquake Engineering, Japan Society of Civil Engineers, 1993;No. 471/I-24:1-12.
- [11] Li VC. On Engineered Cementitious Composites (ECC) -A review of the material and its applications. Journal of Advanced Concrete Technology, 2003;1(3):215-230.
- [12] Li VC, Wang S, Wu C. Tensile strain-hardening behavior of polyvinyl alcohol engineered cementitious composite (PVA-ECC). ACI Materials Journal, 2001;98(6): 483-492.
- [13] Kim YY, Fischer G, Li VC. Performance of bridge deck link slabs designed with ductile ECC. ACI Structural Journal, 2004;101(6):792-801.
- [14] Li VC. Integrated structures and materials design. Materials and Structures, 2007;40(4):387-396.
- [15] Suthiwarapirak P, Matsumoto T, Kanda T. Flexural fatigue failure characteristics of an engineered cementitious composite and polymer cement mortars. Journal of Materials, Concrete Structures and Pavements, Japan Society of Civil Engineers, 2002;No. 718/V-57:121-134.
- [16] Matsumoto T, Suthiwarapirak P, Kanda T. Mechanisms of multiple cracking and fracture of DFRCCs under fatigue flexure. Journal of Advanced Concrete Technology, Japan Concrete Institute, 2003;1(3):299-306.

- [17] Suthiwarapirak P, Matsumoto T, Kanda T. Multiple cracking and fiber bridging characteristics of engineered cementitious composites under fatigue flexure. *Journal of Materials in Civil Engineering*, 2004;16(5):433-443.
- [18] Matsumoto T, Chon P, Suthiwarapirak P. Effect of fiber fatigue rupture on bridging stress degradation of fiber reinforced cementitious composites. *FRAMCOS-5: Proceedings of the Fifth International Conference on Fracture Mechanics of Concrete and Concrete Structures*, Vol. 2. Li VC, Leung CKY, Willam KJ, Billington SL, editors. 2004, pp. 653-660.
- [19] Suthiwarapirak P, Matsumoto T. Fiber bridging degradation based fatigue analysis of ECC under flexure. *Journal of Applied Mechanics*, Japan Society of Civil Engineers, 2003;6:1179-1188.
- [20] Li VC, Matsumoto T. Fatigue crack growth analysis of fiber reinforced concrete with effect of interfacial bond degradation. *Journal of Cement and Concrete Composites*, 1998;20(5):339-351.
- [21] Matsumoto T, Li VC. Fatigue life analysis of fiber reinforced concrete with a fracture mechanics based model. *Journal of Cement and Concrete Composites*, 1999;21(4):249-261.
- [22] Matsumoto T, Li VC. Uniaxial cyclic behavior of discontinuous fiber reinforced composites. *Proceedings of ASCE 4th Materials Engineering Conference*, Chong KP, editors. 1996, pp. 426-435.
- [23] Wu HC, Matsumoto T, Li VC. Buckling of bridging fibres in composites. *Journal of Materials Science Letters*, 1994;13:1800-1803.

## Figure captions

Fig. 1. Shape and dimensions of specimens.

Fig. 2. Experimental set-up. Strain gauge is attached on each of side surfaces.

Fig. 3. Tension-compression loading sequence and crack behaviors.

Fig. 4. Tensile behaviors of Mix A specimens.

Fig. 5. Tensile behaviors of Mix B specimens.

Fig. 6. Multiple cracks of Mix A (left) and Mix B (right). Cracks are visualized with markings.

Fig. 7 Hysteresis curves during tension-compression fatigue of a Case 1 specimen.

Fig. 8 Bridging stress degradation curves during tension-compression fatigue.

Fig. 11 Fitting curve and bridging stress degradation curves of Case 1.

Fig. 12 Fitting curve and bridging stress degradation curves of Case 2.

Fig. 13 Fitting curve and bridging stress degradation curves of Case 3.

Fig. 9 Failure surface of a static tensile specimen with protruded fibers (up) and a tension-compression fatigue (Case 1) specimen without protruded fibers (down).

Fig. 10 Buckling of a fiber and short protrusion of fibers.

Fig. 14 Fitting curve and bridging stress degradation curves during tensile fatigue with maximum tensile strain of 0.1 %.

Fig. 15 Fitting curve and bridging stress degradation curves during tensile fatigue with maximum

tensile strain of 0.15 %.

Fig. 16 Fitting curve and bridging stress degradation curves during tensile fatigue with maximum

tensile strain of 0.2 %.

## Tables

**Table 1 Properties of PVA fibers**

Type	Diameter (mm)	Length (mm)	Volume fraction (%)
PVA	0.04	12	2

**Table 2 Mix proportion**

Water to binder ratio	Fine aggregate to binder ratio	Unit quantity of water (kg/m <sup>3</sup> )
0.32	0.41	360

**Table 3 Experimental cases**

Case	Mix	Number of specimens for static tension	Number of specimens for fatigue	Maximum compressive strain in fatigue (%)	Maximum tensile strain in fatigue (%)
1	A	5	2	0.05	0.2
2	A		2	0	0.2
3	B	2	2	0.05	0.2

**Table 4 Parameters of the fitting curves.**

Case	m	$N_o$ (cycles)	$a_1$	$a_2$	$b_2$
1	25	355	1/25	1/25	0.18
2	9	209	1/30	1/30	0.18
3	12	347	1/30	1/30	0.18

**Table 5 Parameters of the fitting curves.**

Case	m	$N_o$ (cycles)	$a_1$	$a_2$	$b_2$
0.1 %	8	39811	1/15	0	0.2
0.15 %	5.7	63096	1/15	0	0.2
0.2 %	8	31623	1/20	0	0.33